Cerebral Cortex, January 2018;28: 307–322

doi: 10.1093/cercor/bhx285
Advance Access Publication Date: 31 October 2017
Original Article

ORIGINAL ARTICLE

Pathway-Specific Control of Striatal Neuron Vulnerability by Corticostriatal Cannabinoid CB_1 Receptors

Andrea Ruiz-Calvo[1,2], Irene B. Maroto[1,2], Raquel Bajo-Grañeras[1,2], Anna Chiarlone[1,2], Ángel Gaudioso[2], José J. Ferrero[3], Eva Resel[1,2], José Sánchez-Prieto[3], José A. Rodríguez-Navarro[2], Giovanni Marsicano[4], Ismael Galve-Roperh[1,2], Luigi Bellocchio[4] and Manuel Guzmán[1,2]

[1]Centro de Investigación Biomédica en Red sobre Enfermedades Neurodegenerativas (CIBERNED), Instituto Universitario de Investigación Neuroquímica (IUIN) and Department of Biochemistry and Molecular Biology I, Complutense University, 28040 Madrid, Spain, [2]Instituto Ramón y Cajal de Investigación Sanitaria (IRYCIS), 28034 Madrid, Spain, [3]Instituto Universitario de Investigación Neuroquímica (IUIN) and Department of Biochemistry and Molecular Biology IV, Complutense University, 28040 Madrid, Spain and [4]INSERM and University of Bordeaux, NeuroCentre Magendie, Physiopathologie de la Plasticité Neuronale, U1215, 33077 Bordeaux, France

Address correspondence to Manuel Guzmán, Department of Biochemistry and Molecular Biology I, School of Biology, Complutense University, Calle José Antonio Novais 12, 28040 Madrid, Spain. Email: mguzman@quim.ucm.es; Luigi Bellocchio, INSERM, NeuroCentre Magendie, Physiophatologie de la Plasticité Neuronale, U1215, 33077 Bordeaux, France. Email: luigi.bellocchio@inserm.fr

Luigi Bellocchio and Manuel Guzmán contributed equally to supervising this work

Abstract

The vast majority of neurons within the striatum are GABAergic medium spiny neurons (MSNs), which receive glutamatergic input from the cortex and thalamus, and form two major efferent pathways: the direct pathway, expressing dopamine D_1 receptor (D_1R-MSNs), and the indirect pathway, expressing dopamine D_2 receptor (D_2R-MSNs). While molecular mechanisms of MSN degeneration have been identified in animal models of striatal damage, the molecular factors that dictate a selective vulnerability of D_1R-MSNs or D_2R-MSNs remain unknown. Here, we combined genetic, chemogenetic, and pharmacological strategies with behavioral and neurochemical analyses, and show that the pool of cannabinoid CB_1 receptor (CB_1R) located on corticostriatal terminals efficiently safeguards D_1R-MSNs, but not D_2R-MSNs, from different insults. This cell-specific response relies on the regulation of glutamatergic signaling, and is independent from the CB_1R-dependent control of astroglial activity in the striatum. These findings define cortical CB_1R as a pivotal synaptic player in dictating a differential vulnerability of D_1R-MSNs versus D_2R-MSNs, and increase our understanding of the role of coordinated cannabinergic-glutamatergic signaling in establishing corticostriatal circuits and its dysregulation in neurodegenerative diseases.

Key words: Cannabinoid receptor, corticostriatal projection, huntingtin, medium spiny neuron, neuroprotection

Introduction

The striatum is a key node for many vital neurobiological processes such as motor activity, cognitive functions, and affective processes. A very large fraction (*ca*. 95%) of neurons within the striatum are GABAergic medium spiny neurons (MSNs), which receive glutamatergic inputs from the cortex and thalamus. MSNs differ in their neurochemical composition and form 2 major efferent pathways: the direct (striatonigral) pathway and the indirect (striatopallidal) pathway (Kreitzer 2009). MSNs in the direct pathway (herein referred to as D_1R-MSNs) express markers such as dopamine D_1 receptor (D_1R) and substance P, and project mainly to the substantia nigra pars reticulata and the internal segment of the globus pallidus, while MSNs in the indirect pathway (herein referred to as D_2R-MSNs) express markers such as dopamine D_2 receptor (D_2R) and enkephalin, and project mainly to the external segment of the globus pallidus, which, in turn, projects to the subthalamic nucleus. A large number of molecular and cellular mechanisms that lead to the degeneration of MSNs has been defined in preclinical models of striatal damage (Mitchell and Griffiths 2003; Han et al. 2010; Rikani et al. 2014). However, a key unanswered question for understanding the pathobiology of MSNs is what precise molecular and cellular factors can dictate a selective susceptibility of D_1R-MSNs or D_2R-MSNs to neurotoxic stimuli. Although the basic electrophysiological properties of D_1R-MSNs and D_2R-MSNs are rather similar, in general D_2R-MSNs (1) are intrinsically more excitable, (2) have fewer primary dendrites and thus a smaller dendritic surface area, and (3) display a higher frequency of spontaneous excitatory postsynaptic currents and a unique pattern of large-amplitude excitatory events, all of which supports the notion that D_2R-MSNs may be cell-autonomously more susceptible than D_1R-MSNs to damaging excitatory inputs (Kreitzer 2009; Raymond et al. 2011). Huntington's disease (HD), the archetypical neurodegenerative disease that originates primarily from the damage of MSNs, is characterized by differential alterations in the two MSN populations that occur at different stages of disease progression. Thus, based on studies conducted on both mouse models of HD and postmortem brain samples from HD patients, the classical view defines that D_2R-MSNs are affected at earlier stages of the disease and to a greater extent than D_1R-MSNs, which is consistent with the notion that early-onset chorea-like movements result from a preferential dysfunction/loss of D_2R-MSNs, while later-onset bradykinesia and dystonia are a consequence of an additional dysfunction/loss of D_1R-MSNs (Walker 2007; Han et al. 2010; Ross et al. 2014).

However, there is also some evidence for the occurrence of early alterations in D_1R-MSNs in both patients (Hedreen and Folstein 1995) and mouse models of HD (Andre et al. 2011). Accordingly, D_1R activation enhances NMDAR-evoked excitotoxic signaling on MSNs, while D_2R activation usually reduces NMDAR-dependent responses (Chen et al. 2013; Sepers and Raymond 2014). For example, D_1R engagement has been shown to potentiate glutamate-mediated excitotoxic signaling to provoke the death of MSNs (Cepeda and Levine 1998; McLaughlin et al. 1998; Zeron et al. 2002; Tang et al. 2007; Paoletti et al. 2008; Chen et al. 2013), while cocaine (Go et al. 2010) and methamphetamine (Jayanthi et al. 2002) administration, by overstimulating D_1R-mediated signaling, damage MSNs at least in part by converging with glutamatergic overactivation. This evidence suggests exclusive protective mechanisms on D_1R-MSNs that would spare them—compared with D_2R-MSNs- in HD. Here, we tested the hypothesis that the cannabinoid CB_1 receptor (CB_1R) drives such a differential protection of D_1R-MSNs versus D_2R-MSNs. CB_1R, the main target of endocannabinoids and the cannabis active ingredient Δ9-tetrahydrocannabinol, is one of the most abundant metabotropic receptors in the basal ganglia, where it mediates inhibition of presynaptic activity (Glass et al. 2000; Katona and Freund 2008; Atwood et al. 2014). In particular, CB_1R (1) is expressed on both MSNs and corticostriatal projections (Katona and Freund 2008), (2) plays a key role in the striatal control of motor behavior (Kreitzer 2009; Castillo et al. 2012), and (3) protects MSNs in animal models of excitotoxicity (Fernandez-Ruiz et al. 2011) and HD (Blazquez et al. 2011; Mievis et al. 2011; Chiarlone et al. 2014). By combining a wide array of genetic, chemogenetic and pharmacological strategies with behavioral and neurochemical analyses, we show that CB_1R located on corticostriatal projections, by blunting glutamatergic output, selectively safeguards D_1R-MSNs of the mouse dorsal striatum.

Materials and Methods

Animals

We used conditional mutant mice, generated by the Cre-*loxP* technology, in which the CB_1R gene is primarily absent from cortical glutamatergic neurons of the dorsal telencephalon ($CB_1R^{floxed/floxed;Nex\text{-}Cre/+}$ mice; herein referred to as Glu-$CB_1R^{-/-}$ mice) (Monory et al. 2006) or from astroglial cells ($CB_1R^{floxed/floxed;GFAP\text{-}CreERT2/+}$ mice; herein referred to as glial fibrillary acidic protein (GFAP)-$CB_1R^{-/-}$ mice; treated with tamoxifen to induce Cre expression as described) (Han et al. 2012). We also used BAC transgenic mice expressing the tdTomato and EGFP reporter genes under the control of the D_1R and D_2R promoter, respectively (*Drd1a*-tdTomato/*Drd2*-EGFP mice; colony founders kindly provided by Dr. Rosario Moratalla, Cajal Institute, Madrid, Spain) (Suarez et al. 2014). Hemizygous mice transgenic for exon 1 of the human huntingtin gene with a largely expanded CAG tract (~250 CAG repeats; R6/2 L mice) were generated from R6/2 mice (The Jackson Laboratory) and subsequently crossed with $CB_1R^{floxed/floxed}$ mice to obtain the R6/2 L:$CB_1R^{floxed/floxed}$ double-mutant line as described (Chiarlone et al. 2014). In all experiments, mutant mice were compared with their corresponding littermates. Wild-type C57BL/6 N mice were purchased from Harlan Laboratories. Animal housing, handling and assignment to the different experimental groups were conducted as described (Blazquez et al. 2011). Except for the experiments conducted with the R6/2 L:$CB_1R^{floxed/floxed}$ line (see Fig. 4), all animals used were male adults (*ca*. 8 week-old). Adequate measures were taken to minimize pain or discomfort of the animals. Mice were sacrificed by intracardial perfusion and their brains were excised for tissue analyses. All the experimental procedures used were performed in accordance with the guidelines and with the approval of the Animal Welfare Committee of Universidad Complutense de Madrid and Comunidad de Madrid, and in accordance with the directives of the European Commission.

Viral Vectors

Constructs expressing CFP-tagged human huntingtin exon 1 harboring a pathogenic polyQ tract of 94 CAG repeats or a normal, non-pathogenic polyQ tract of 16 CAG repeats (Maynard et al. 2009) (kindly provided by Dr. José J. Lucas, Severo Ochoa Molecular Biology Center, Madrid, Spain); HA-tagged Cre recombinase (Monory et al. 2006); EGFP (Chiarlone et al. 2014); G_q-coupled human M_3 muscarinic DREADD (hM3Dq) fused to

mCherry (Alexander et al. 2009) (kindly provided by Dr. Brian L. Roth, University of North Carolina, Chapel Hill, NC) or mCherry were subcloned in rAAV expression vectors with a minimal CaMKIIα promoter (kindly provided by Dr. Karl Deisseroth, Stanford University, Stanford, CA, USA) by using standard molecular cloning techniques. CFP-tagged polyQ constructs were also subcloned in rAAV expression vectors with a minimal GFAP promoter. All vectors used were of an AAV1/AAV2 mixed serotype, and were generated by calcium phosphate transfection of HEK293T cells and subsequent purification (Monory et al. 2006). Vectors were injected stereotactically either into the dorsal striatum (vectors diluted in 3 µL PBS) or into the motor cortex projecting onto the dorsal striatum (vectors diluted in 1.5 µL PBS). In the case of the striatum, each animal received one bilateral injection at coordinates (mm to bregma): antero-posterior +0.5, lateral ±2.0, dorso-ventral −3.5. In the case of the cortex, each animal received 2 bilateral injections at coordinates (mm to bregma): antero-posterior +1.5, lateral ±1.2, dorso-ventral −1.7; and antero-posterior −0.5, lateral ±1.2, dorso-ventral −1.2. We have described previously the placement of the rAAV vectors within the cortex and the striatum under those conditions (Chiarlone et al. 2014; Blazquez et al. 2015; Bellocchio et al. 2016). In the DREADD experiments (Chiarlone et al. 2014), 8 week-old animals were injected with the rAAV vector, then left untreated for 6 weeks, and subjected to the pharmacological treatments for 4 weeks. Finally, RotaRod test was conducted and animals were subsequently sacrificed. In the R6/2 L:$CB_1R^{floxed/floxed}$ mouse experiments (Chiarlone et al. 2014), 4 week-old animals were injected with the rAAV vectors and, at week 20 of age, RotaRod test was conducted and animals were subsequently sacrificed.

Drugs

CNO (Santa Cruz Biotechnology) was prepared in saline (0.9% NaCl) just before the experiments and injected i.p. at 10 mg/kg/day. SR141716 (rimonabant; kindly provided by Sanofi-Aventis, Montpellier, France) was stored in DMSO. Just before the experiments, solutions of vehicle [1% (v/v) DMSO in Tween-20/saline (1:18, v/v)] and SR141716 (1 mg/kg/day) were prepared for i.p. injections. Stock solution of MK-801 (Sigma) was prepared in DMSO and, just before the experiments, diluted in saline (final DMSO concentration: 2%) for i.p. injections (0.03 mg/kg/day). SKF-81297 (Tocris) was prepared fresh in saline just before the experiments and injected i.p. at 1 mg/kg.

Confocal Microscopy

Coronal free-floating sections (30 µm-thick) were obtained from paraformaldehyde-perfused mouse brains. Samples were incubated with antibodies against NeuN (1:500; Chemicon #MAB377), DARPP-32 (1:1000; BD #611520), D_1R (1:500; Frontier Science #af500), D_2R (1:500; Frontier Science #af750), S100β (1:500; Abcam #ab868) or GFAP-Cy3 (1:1000; Sigma #C 9205), followed by staining with the corresponding Alexa Fluor 488, 594 or 647 antibodies as appropriate (1:1000; Life Technologies). Nuclei were visualized with DAPI. Analysis of marker-protein immunoreactivity in the dorsal striatum was conducted as described (Bellocchio et al. 2016) in a 1-in-10 series per animal (from bregma +1.5 to −0.5 coronal coordinates). For DARPP-32, D_1R and D_2R, data were calculated as immunoreactive area per total cell nuclei, and expressed as percentage of the control. For NeuN, as well as for tdTomato and EGFP fluorescence in *Drd1a*-tdTomato/*Drd2*-EGFP mice, data were calculated as number of positive cells per total cell nuclei, and expressed as percentage of the control. Confocal fluorescence images were acquired using TCS-SP2 software and a SP2 AOBS microscope (Leica). Images were analyzed with ImageJ software (NIH).

Behavior

Motor coordination (RotaRod performance) was evaluated along 3 consecutive days as described (Bellocchio et al. 2016). Ambulation analyses were conducted in an automated actimeter (ActiTrack; Panlab), as described (Bellocchio et al. 2016), after acute (30 min) treatment with vehicle or SKF-81297 (1 mg/kg, i.p.). Specifically, one day after termination of chronic pharmacological treatments and RotaRod assays, half of the animals within each experimental group was injected with vehicle, the other half was injected with SKF-81297, and ambulation was measured. The day after, the treatments were crossed-over and ambulation was measured again. For each animal, SKF-81297-induced ambulation over vehicle-induced ambulation (in cm) was determined.

Microdialysis

Extracellular concentrations of glutamate and GABA were measured in the dorsal striatum of 8 week-old Glu-$CB_1R^{-/-}$ mice and their $CB_1R^{floxed/floxed}$ littermates by brain microdialysis in vivo (Rodriguez-Navarro et al. 2009). The active area of the microdyalisis probe (CMA Microdyalisis AB) was implanted in the striatum at coordinates: 0.5 mm caudal to bregma, 2 mm lateral to midline, 3.5 mm below the dura. The probes were perfused with a standard or modified KRB solution (122 mM NaCl, 3 mM KCl, 0.4 mM KH_2PO_4, 1.2 mM $MgSO_4$, 25.2 mM $NaHCO_3$, 1.2 mM $CaCl_2$) at a flow rate of 2 µL/min with a syringe minipump (Bionalytical Systems). A perfusion period of 90 min without sampling was conducted to enable the recovery of basal amino acid levels after probe implantation. Then, perfusate samples were collected every 15 min and stored at −80 °C until analysis. For amino acid determinations, dialysates were derivatized with *ortho*-phthaldialdehyde. The fluorescent derivatized amino acids were separated by reversed-phase chromatography on a Micra C18 column (33-3-4.6 mm, particle size 1.5 mm) by gradient elution. The mobile phase consisted of solvent A (50 mM sodium acetate, pH 5.88) and solvent B (methanol) with a binary gradient. Solvent flow rate was adjusted to 0.5 mL/min, and the injection volume was 10 µL. Fluorescence detection (Perkin-Elmer LS4) was performed at 365 and 455 nm for excitation and emission wavelengths, respectively. Amino acids were identified by their retention times, and their concentrations were calculated by comparing them to calibrated amino acid external standard solutions (1.5 µM).

Synaptosomes

Striatal synaptosomes were isolated from 8 week-old Glu-$CB_1R^{-/-}$ and $CB_1R^{floxed/floxed}$ mice, and used for KCl-induced glutamate release experiments as described (Martin et al. 2010; Chiarlone et al. 2014).

Statistics

Data are presented as mean ± SEM. Statistical comparisons were made by 1-way or 2-way ANOVA with Bonferroni, Tukey, Neuman-Keuls or Sidak post hoc test, or by unpaired Student's

t-test, as appropriate. A *P*-value of <0.05 was considered significant. Graphs and statistics were generated by GraphPad Prism 6.0.

Results

D_1R-MSNs and D_2R-MSNs are Equally Vulnerable to Cell-Autonomous Mutant Huntingtin-Induced Damage

To evaluate the potentially different vulnerability of D_1R-MSNs and D_2R-MSNs to huntingtin-induced damage we first used a rAAV-vector delivery strategy based on the expression of CFP-tagged human huntingtin exon 1 harboring a pathogenic polyQ tract of 94 CAG repeats (herein used as a model of mutant huntingtin, mtHtt) or a normal, non-pathogenic polyQ tract of 16 CAG repeats (herein used as a model of wild-type huntingtin, wtHtt). The expression of the transgene was driven by a minimal calcium/calmodulin-dependent protein kinase II-α (CaMKIIα) promoter in order to confine it to the main cell populations affected in HD, namely MSNs (when viral injections were performed into the dorsal striatum) or cortical glutamatergic neurons (when viral injections were performed into the motor cortex). Viral inoculation was conducted in BAC transgenic mice expressing the tdTomato and EGFP reporter genes under the control of the D_1R or D_2R promoter, respectively (Fig. 1A). The extent of wtHtt or mtHtt transgene expression at the time points used in the study was comparable between striatum and cortex, and, within the striatum, between D_1R-MSNs and D_2R-MSNs (Supplementary Fig. S1A–E).

Expression of mtHtt in MSNs of the dorsal striatum for 2 weeks produced a remarkable loss of the *pan*-neuronal marker NeuN and the *pan*-MSN marker dopamine- and cAMP-regulated phosphoprotein of 32 kDa (DARPP-32), as well as a parallel reduction of cells that were positive for tdTomato fluorescence (*i.e.*, D_1R-MSNs) or EGFP fluorescence (i.e., D_2R-MSNs) (Fig. 1B,C). This observation was supported by conducting immunofluorescence experiments with antibodies raised against each of the two receptors (Fig. 1B,C). Of note, D_1R-MSNs and D_2R-MSNs were equally vulnerable to mtHtt-induced damage (Fig. 1B,C). Moreover, this loss of MSN markers had a notable functional impact as evidenced by the impairment of RotaRod performance, a well-established motor coordination paradigm that relies, at least largely, on striatal function (Fig. 1B). In contrast to this damaging effect of mtHtt expressed by MSNs in situ, no significant loss of neuronal markers or decline in RotaRod performance was observed when mtHtt was selectively expressed in principal neurons of the motor cortex, either 2 weeks (data not shown) or even 4 weeks after viral injection (Fig. 1D).

Taken together, these data indicate that D_1R-MSNs and D_2R-MSNs are equally sensitive to cell-autonomous mtHtt-induced toxicity, and that expression of mtHtt in cortical principal neurons is not sufficient *per se* to produce a significant damage of MSNs.

Expression of Mutant Huntingtin in the Cortex Damages D_1R-MSNs but not D_2R-MSNs upon CB_1R Pharmacological Blockade

It is not known whether CB_1R-evoked neuroprotection may be selective for different MSN populations, and, if so, which precise population(s) of CB_1R molecules would be involved in such effect. To evaluate this question we first injected -as above- CaMKIIα promoter-driven wtHtt or mtHtt-expressing rAAV vectors into the dorsal striatum or motor cortex of D_1R-tdTomato/D_2R-EGFP reporter mice, and subsequently treated the mice with vehicle or the CB_1R-selective antagonist SR141716 (rimonabant) at 1 mg/kg/day (i.p.) for 2 weeks (viral inoculation into the striatum) or 4 weeks (vital inoculation into the cortex) (Fig. 2A). Rimonabant did not affect striatum-autonomous mtHtt-mediated loss of D_1R-MSN or D_2R-MSN markers, nor worsened motor coordination deficits under these conditions (Fig. 2B). In remarkable contrast, CB_1R pharmacological blockade aggravated those hallmarks of striatal integrity when mtHtt was selectively expressed in principal neurons of the motor cortex (Fig. 2C). Moreover, MSN damage under these conditions exclusively involved D_1R-MSNs, while D_2R-MSNs remained unaffected (Fig. 2C).

Taken together, these observations support that, when CB_1R activity is compromised, expression of mtHtt in cortical principal neurons determines a dissimilar susceptibility to damage of D_1R-MSNs versus D_2R-MSNs.

CB_1R Located on Corticostriatal Projections Protects D_1R-MSNs but not D_2R-MSNs from Cortex-Elicited Damage

To provide further support to the aforementioned notion we used three different experimental paradigms in which cortical CB_1R function and neuronal activity were manipulated in vivo in a spatiotemporally-selective manner.

In a first experimental paradigm we injected conditional mutant mice bearing a genetic deletion of CB_1R in dorsal telencephalic glutamatergic neurons ($CB_1R^{floxed/floxed;Nex\text{-}Cre/+}$ mice; herein referred to as Glu-$CB_1R^{-/-}$ mice) (Monory et al. 2006), and $CB_1R^{floxed/floxed}$ control littermates, with CaMKIIα promoter-driven wtHtt or mtHtt-expressing rAAV vectors into the motor cortex (Fig. 3A). As above, no significant mtHtt-evoked striatal toxicity was observed in control mice (Fig. 3B,C). In contrast, cortical mtHtt induced a neurotoxic effect on the striatum of Glu-$CB_1R^{-/-}$ mice, as determined by a loss of striatal DARPP-32 expression as well as a decline in RotaRod performance (Fig. 3B). Remarkably, and in line with the rimonabant experiment on D_1R-tdTomato/D_2R-EGFP reporter mice described above, the impact of cortical mtHtt expression on Glu-$CB_1R^{-/-}$ mice involved D_1R-MSNs exclusively, while D_2R-MSNs remained intact (Fig. 3C).

In a second experimental paradigm, we crossed R6/2L mice, a transgenic model of HD that systemically expresses exon 1 of the human huntingtin gene comprising a largely expanded CAG tract, with $CB_1R^{floxed/floxed}$ mice, thus generating a R6/2L:$CB_1R^{floxed/floxed}$ line, that allows the spatiotemporally-controlled excision of the *loxP*-flanked CB_1R gene by Cre recombinase (Chiarlone et al. 2014). These R6/2L:$CB_1R^{floxed/floxed}$ animals (and $CB_1R^{floxed/floxed}$ littermates) were injected into the dorsal striatum or the motor cortex with a rAAV-vector encoding Cre (or EGFP) under the control of the CaMKIIα promoter (Fig. 4A). We had previously shown that, under these conditions, CB_1R gene inactivation in the motor cortex –but not the dorsal striatum- of R6/2 L:$CB_1R^{floxed/floxed}$ mice reduced striatal DARPP-32 expression and RotaRod performance (Chiarlone et al. 2014). As shown in Fig. 4B, this procedure of selective CB_1R gene inactivation in dorsal-striatum MSNs did not affect D_1R-MSNs or D_2R-MSNs expression. In contrast, selective CB_1R gene inactivation in cortical principal neurons impacted D_1R-MSNs, while D_2R-MSNs were not affected (Fig. 4C).

In a third experimental paradigm, we sought to extrapolate the above observations on cortical mtHtt-induced striatal

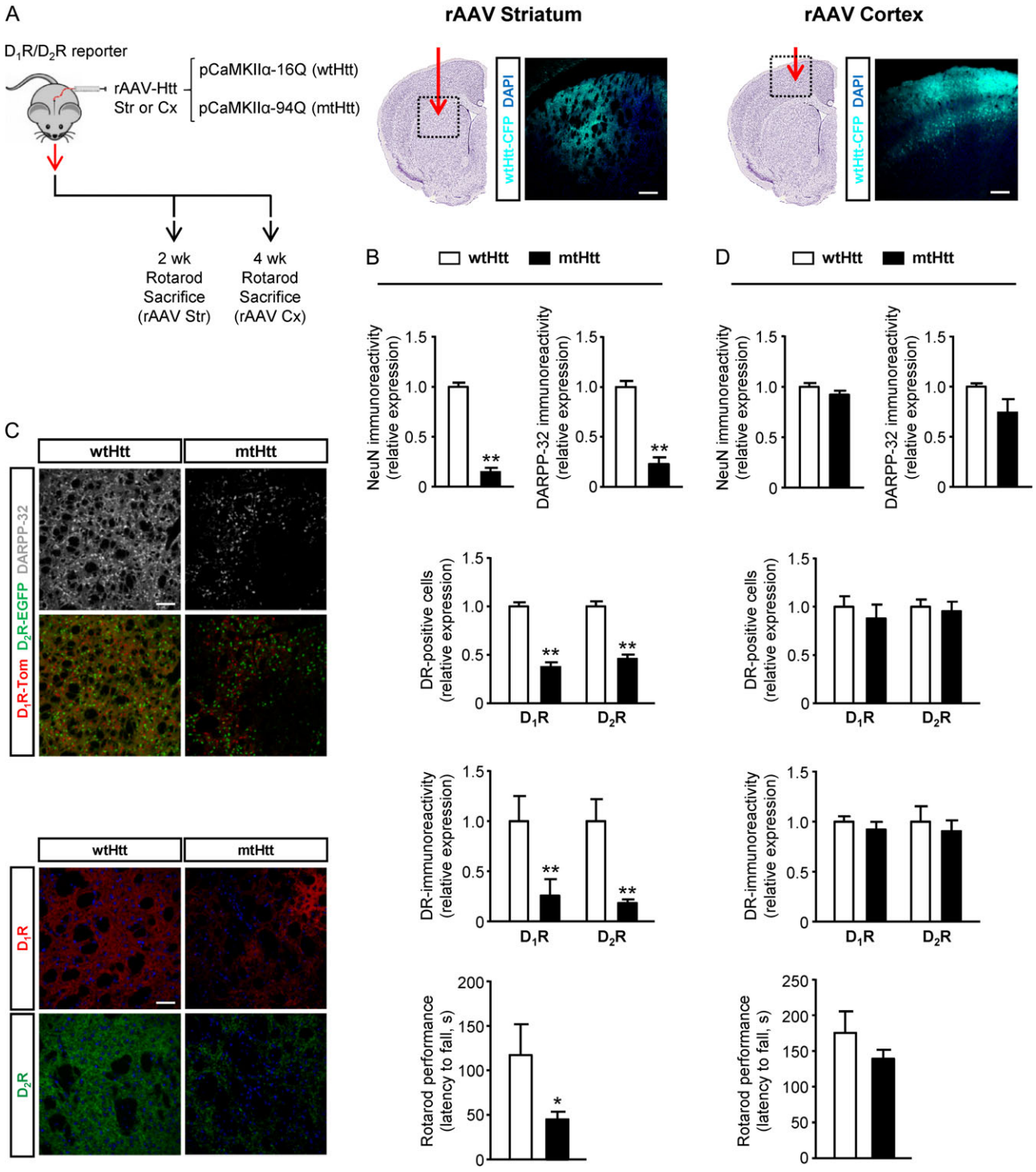

Figure 1. D_1R-MSNs and D_2R-MSNs are equally vulnerable to cell-autonomous mutant huntingtin-induced damage. *Drd1a*-tdTomato/*Drd2*-EGFP mice were injected stereotactically into the dorsal striatum or the motor cortex with rAAV vectors encoding wtHtt (16Q-CFP) or mtHtt (94Q-CFP) under the control of a CaMKIIα promoter. *A*, Scheme of the experiment. Representative examples of brain hemispheres expressing the wtHtt vector in the striatum or the cortex. The dotted lines depict the infected areas. Scale bar, 200 μm. *B*, NeuN and DARPP-32 immunoreactivity, tdTomato (D_1R) fluorescence and EGFP (D_2R) fluorescence, as well as D_1R and D_2R immunoreactivity in the dorsal striatum, together with RotaRod performance (time to fall), 2 weeks after viral inoculation into the striatum. *C*, Representative images. Scale bar, 100 μm (upper panels) or 50 μm (lower panels). *D*, NeuN and DARPP-32 immunoreactivity, tdTomato (D_1R) fluorescence and EGFP (D_2R) fluorescence, as well as D_1R and D_2R immunoreactivity in the dorsal striatum, together with RotaRod performance (time to fall), 4 weeks after viral inoculation into the cortex. Data of neuronal markers are expressed as relative values of the wtHtt group. $^*P < 0.05$, $^{**}P < 0.01$ from the corresponding wtHtt group ($n = 6$–8 animals per group).

damage to another model of cortex-initiated striatal damage. Thus, we selectively enhanced neuronal activity with a designer receptor exclusively activated by designer drug (DREADD). This chemogenetic technique is based on the expression of engineered GPCRs that are selectively activated by systemically bioavailable, brain-penetrant and otherwise

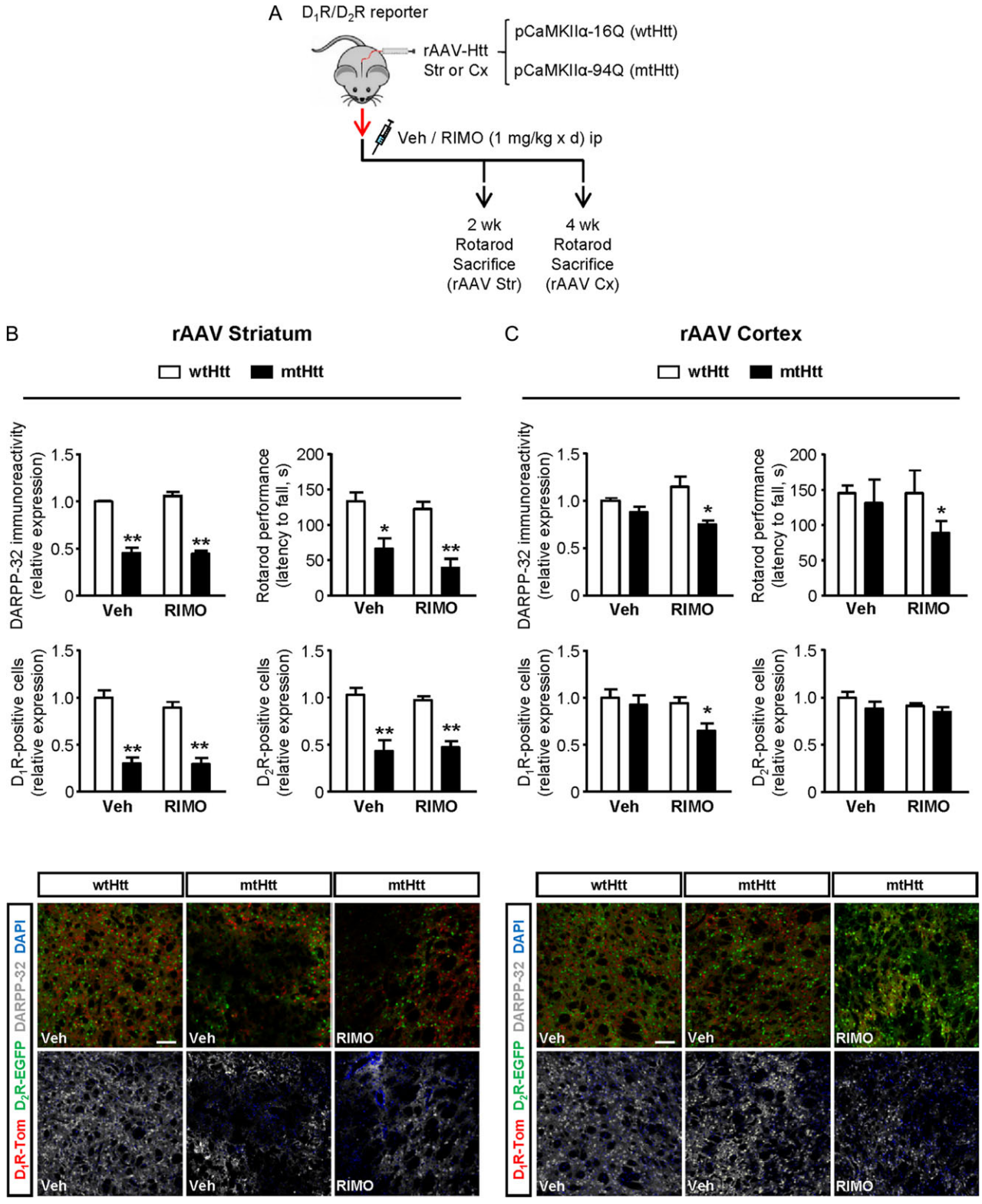

Figure 2. Expression of mutant huntingtin in the cortex damages D_1R-MSNs but not D_2R-MSNs upon CB_1R pharmacological blockade. *Drd1a*-tdTomato/*Drd2*-EGFP mice were injected stereotactically into the dorsal striatum or the motor cortex with rAAV vectors encoding wtHtt (16Q-CFP) or mtHtt (94Q-CFP) under the control of a CaMKIIα promoter. Animals were subsequently treated with vehicle or SR141716 (rimonabant; 1 mg/kg/day, i.p.) for 2 weeks (viral inoculation into the striatum) or 4 weeks (vital inoculation into the cortex). A, Scheme of the experiment. B, DARPP-32 immunoreactivity, tdTomato (D_1R) fluorescence and EGFP (D_2R) fluorescence in the dorsal striatum, as well as RotaRod performance (time to fall), upon viral inoculation into the striatum. C, DARPP-32 immunoreactivity, tdTomato (D_1R) fluorescence and EGFP (D_2R) fluorescence in the dorsal striatum, as well as RotaRod performance (time to fall), upon viral inoculation into the cortex. Data of neuronal markers are expressed as relative values of the wtHtt-vehicle group. Representative images are shown. Scale bar, 100 μm. *$P < 0.05$, **$P < 0.01$ from the corresponding wtHtt-vehicle group ($n = 6$–8 animals per group).

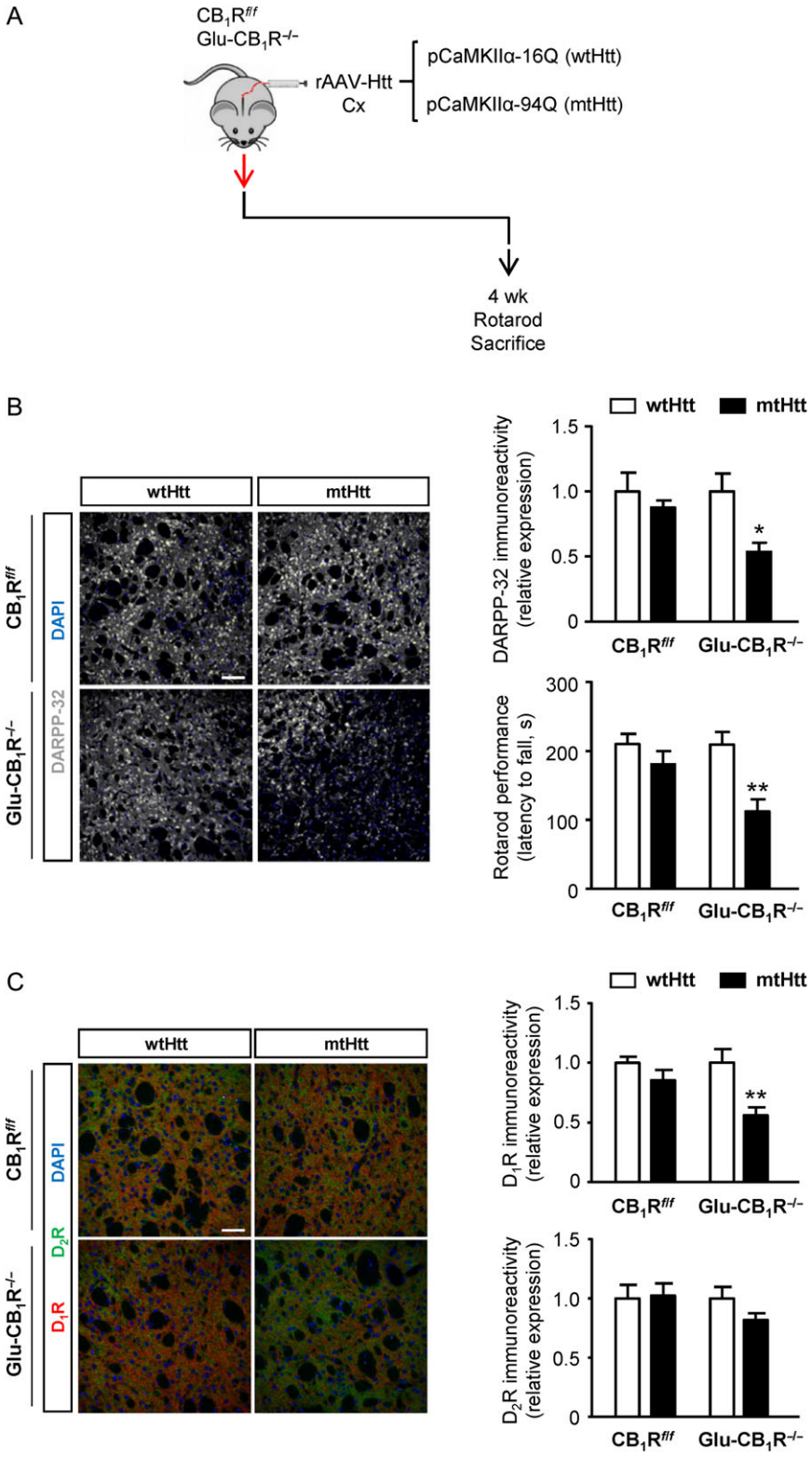

Figure 3. Genetic inactivation of cortical CB_1R enhances the vulnerability of D_1R-MSNs but not D_2R-MSNs to cortical mutant huntingtin-elicited damage. Glu-$CB_1R^{-/-}$ mice and $CB_1R^{floxed/floxed}$ littermates were injected stereotactically into the motor cortex with rAAV vectors encoding wtHtt (16Q-CFP) or mtHtt (94Q-CFP) under the control of a CaMKIIα promoter. A, Scheme of the experiment. B, DARPP-32 in the dorsal striatum and RotaRod performance (time to fall) 4 weeks after viral inoculation. Representative images are shown. Scale bar, 100 μm. C, D_1R and D_2R immunoreactivity in the dorsal striatum 4 weeks after viral inoculation. Representative images are shown. Scale bar, 50 μm. Data of neuronal markers are expressed as relative values of the wtHtt-$CB_1R^{floxed/floxed}$ group. *P < 0.05, **P < 0.01 from the corresponding wtHtt group (n = 8–10 animals per group).

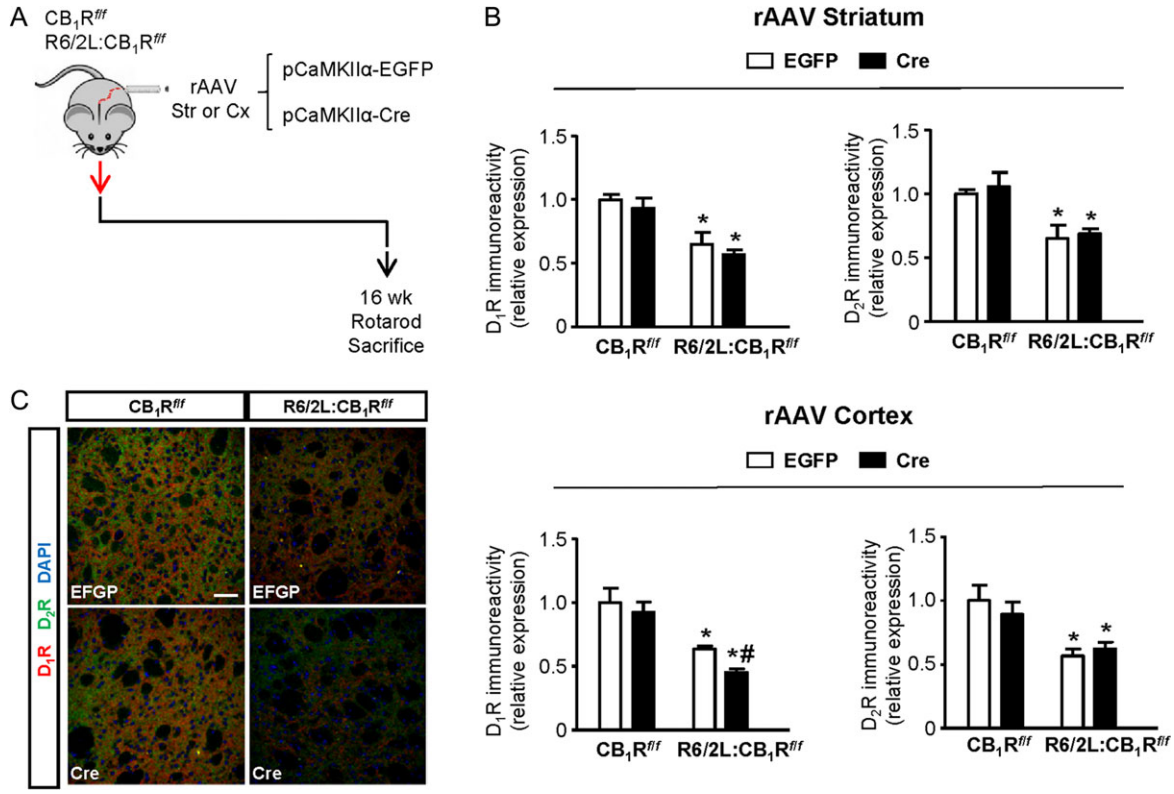

Figure 4. Genetic inactivation of cortical CB_1R enhances the vulnerability of D_1R-MSNs but not D_2R-MSNs in R6/2 mice. Four week-old R6/2 L:$CB_1R^{floxed/floxed}$ mice and $CB_1R^{floxed/floxed}$ littermates were injected stereotactically into the motor cortex or the dorsal striatum with rAAV vectors encoding Cre recombinase or EGFP under the control of a CaMKIIα promoter as previously described (Chiarlone et al. 2014). At week 20 of age, animals were sacrificed for histological analyses. A, Scheme of the experiment. B, D_1R and D_2R immunoreactivity in the dorsal striatum upon viral inoculation into the striatum. C, D_1R and D_2R immunoreactivity in the dorsal striatum upon viral inoculation into the cortex. Representative images are shown. Scale bar, 50 μm. Data are expressed as relative values of the EGFP-$CB_1R^{floxed/floxed}$ group. *P < 0.05 from the corresponding $CB_1R^{floxed/floxed}$ group; #P < 0.05 from the corresponding EGFP-R6/2 L:$CB_1R^{floxed/floxed}$ group (n = 4–6 animals per group).

pharmacologically inert ligands such as clozapine-*N*-oxide (CNO) (Lee et al. 2014). Specifically, wild-type C57BL/6N mice were injected into the motor cortex with a rAAV-vector encoding a G_q protein-coupled DREADD (hM3Dq) fused to mCherry (or only mCherry as control) driven by the CaMKIIα promoter. Animals were subsequently treated with vehicle or CNO in conditions known to evoke sustained cortical activation and thereby excitotoxic damage on the striatum (10 mg/kg/day, i.p. for 4 weeks; Fig. 5A) (Alexander et al. 2009; Chiarlone et al. 2014). In agreement with previous data (Chiarlone et al. 2014; Bellocchio et al. 2016), the effects elicited by CNO in DREADD-expressing mice were specific and not due to an off-target action of the drug (Gomez et al. 2017) as shown by the lack of overt effects in control mCherry-expressing animals (Fig. 5B,C). Moreover, CB_1R pharmacological blockade (rimonabant at 1 mg/kg/day, i.p. for 4 weeks; Fig. 5A) sensitized mice to striatal damage upon prolonged cortical overactivation, and this effect entailed D_1R-MSNs but not D_2R-MSNs (Fig. 5B,C).

Taken together, these findings support that CB_1R located on corticostriatal projections protects D_1R-MSNs but not D_2R-MSNs from damage initiated at cortical principal neurons.

CB_1R Located on Corticostriatal Projections Protects D_1R-MSNs from Cortex-Elicited Damage by Inhibiting Glutamatergic Transmission

To evaluate whether cortical CB_1R controls glutamatergic signaling onto the striatum we first measured by in vivo microdialysis extracellular glutamate concentration in the dorsal striatum of Glu-$CB_1R^{-/-}$ mice and $CB_1^{floxed/floxed}$ littermates. KCl-induced neuronal depolarization enhanced glutamate levels in Glu-$CB_1R^{-/-}$ mice compared to control animals (Fig. 6A). As a control we analyzed in parallel GABA concentration and found no significant change upon cortical CB_1R genetic ablation (Fig. 6A). We subsequently isolated striatal synaptosomes from Glu-$CB_1R^{-/-}$ mice and $CB_1R^{floxed/floxed}$ littermates, and measured glutamate release, thus assessing the action of CB_1R located on corticostriatal terminals. In agreement with the aforementioned microdialysis experiments, KCl-evoked glutamate release from striatal synaptosomes was enhanced upon CB_1R genetic deletion (Fig. 6B).

To assess the functional impact of the CB_1R receptor-mediated control of glutamatergic signaling on striatal integrity in vivo we injected Glu-$CB_1R^{-/-}$ mice and $CB_1R^{floxed/floxed}$ littermates with CaMKIIα promoter-driven wtHtt or mtHtt-expressing vectors into the motor cortex, and treated them with vehicle or the NMDAR-selective antagonist MK-801 at 0.03 mg/kg/day (i.p.) for 4 weeks (Fig. 6C). MK-801 administration rescued the loss of striatal DARPP-32 and D_1R expression, as well as the decline in RotaRod performance, elicited by cortical mtHtt expression in Glu-$CB_1R^{-/-}$ mice (Fig. 6D). As an additional functional readout, we found that cortical mtHtt expression in Glu-$CB_1R^{-/-}$ mice impaired the characteristic stimulant-like pattern on motor activity evoked by acute administration of the D_1R-selective agonist SKF-81297 (1 mg/kg, i.p.), thus pointing to an impact on direct-pathway striatal

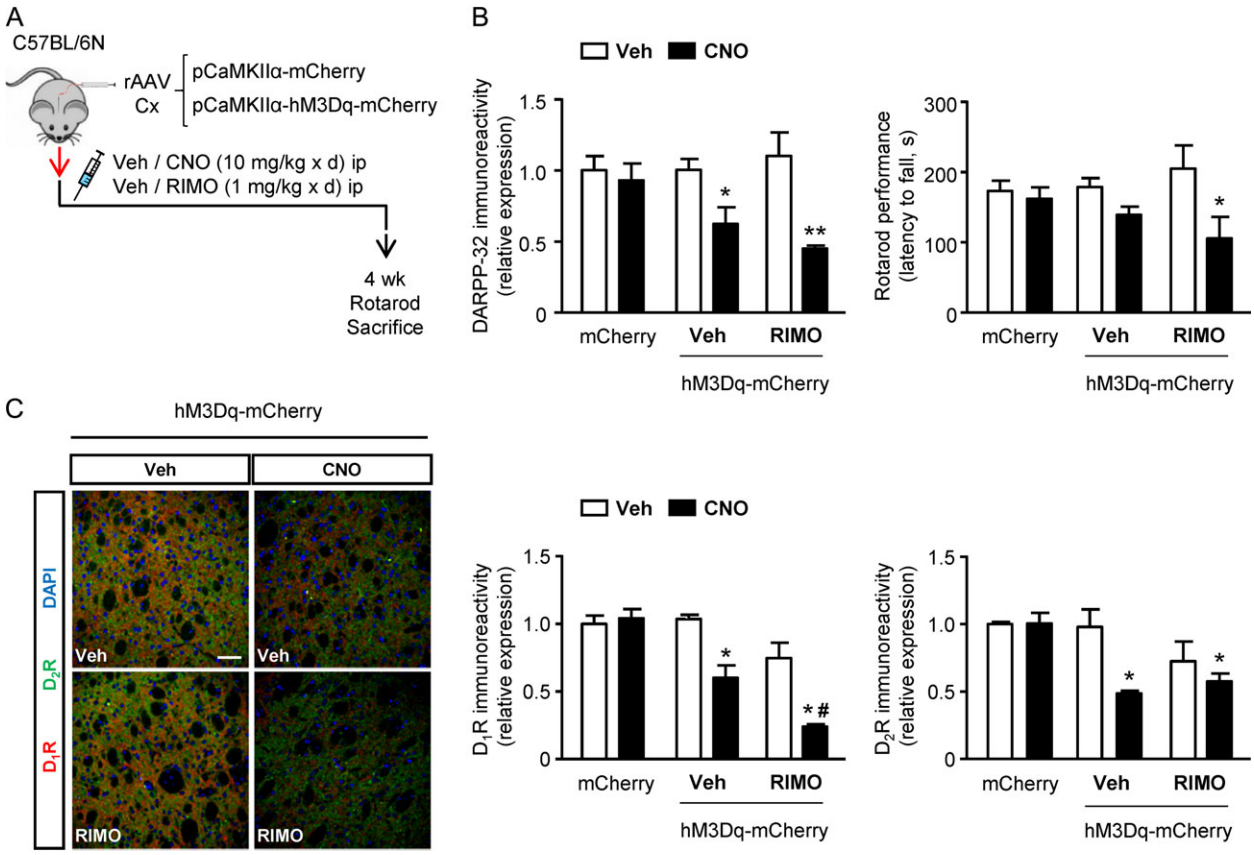

Figure 5. Sustained chemogenetic activation of cortical projections damages D_1R-MSNs but not D_2R-MSNs upon CB_1R pharmacological blockade. Eight week-old C57BL/6 N mice were injected stereotactically into the motor cortex with a rAAV-vector encoding hM3Dq-mCherry (or only mCherry) under the control of a CaMKIIα promoter as previously described (Chiarlone et al. 2014). Six weeks later, animals were treated for 4 weeks with vehicle or CNO (10 mg/kg/day, i.p), alone or in combination with vehicle or SR141716 (rimonabant; 1 mg/kg/day, i.p.). RotaRod performance was evaluated along the last 3 days of treatment, and the next day these 18 week-old animals were sacrificed for histological analyses. *A*, Scheme of the experiment. *B*, DARPP-32 in the dorsal striatum and RotaRod performance (time to fall). *C*, D_1R and D_2R immunoreactivity in the dorsal striatum. Representative images are shown. Scale bar, 50 μm. Data of neuronal markers are expressed as relative values of the mCherry-vehicle group. $^*P < 0.05$, $^{**}P < 0.01$ from the corresponding vehicle-vehicle group; $^{\#}P < 0.05$ from the corresponding vehicle-CNO group (n = 4–6 animals per group).

circuitry (Fig. 6*E*). Of note, this effect was also rescued by MK-801 treatment (Fig. 6*E*).

Taken together, these data support that CB_1R located on corticostriatal projections protects D_1R-MSNs from cortical mtHtt-evoked damage by inhibiting glutamatergic transmission.

CB_1R Located on Corticostriatal Projections Protects D_1R-MSNs from Astroglia-Elicited Damage by Inhibiting Glutamatergic Transmission

Astrocytes are pivotal elements in the control of brain glutamatergic signaling (Murphy-Royal et al. 2017). In HD, mtHtt aggregates accumulate in astrocytes from patients and animal models of the disease, and preclinical evidence supports that this can contribute to drive disease progression, at least in part through alterations in glutamate homeostasis (Benraiss et al. 2016; Jiang et al. 2016; Meunier et al. 2016; Jansen et al. 2017). Moreover, astrocytes express CB_1R, metabolize endocannabinoids, and modulate endocannabinergic transmission (Navarrete and Araque 2010; Stella 2010; Han et al. 2012). Hence, we studied the possible role of astroglial CB_1R on mtHtt-evoked striatal damage. For this purpose we injected into the dorsal striatum of C57BL/6N mice rAAV vectors encoding wtHtt or mtHtt under the control of a minimal GFAP promoter, in order to confine their expression to astrocytes (Fig. 7A). Transgene expression was evident in a large fraction of striatal astrocytes (S100β-positive cells or GFAP-positive cells). Specifically, a ca. 70% of the total wtHtt-CFP-positive cells was found to be also S100β-positive, and a ca. 45% of the total GFAP-positive area was found to be also wtHtt-CFP-positive (Supplementary Fig. S2A–C). Moreover, transgene expression was undetectable in MSNs (DARPP-32-positive cells) (Supplementary Fig. S2A,B). Under these experimental conditions, mtHtt produced, 2 weeks after viral injection, a loss of striatal NeuN, DARPP-32 and D_1R –but not D_2R- immunoreactivity (Fig. 7B), as well as an impairment of motor coordination (Fig. 7C).

To evaluate a possible neuroprotective role of astroglial CB_1R in this setting, conditional mutant mice bearing an inducible genetic deletion of CB_1R in astroglial cells ($CB_1R^{floxed/floxed;\ GFAP\text{-}CreERT2/+}$ mice; herein referred to as GFAP-$CB_1R^{-/-}$ mice) (Han et al. 2012), as well as $CB_1R^{floxed/floxed}$ littermates, were injected with GFAP promoter-driven wtHtt or mtHtt-expressing vectors into the dorsal striatum (Fig. 8A). Selective CB_1R genetic inactivation in astroglial cells did not exacerbate the decline of striatal DARPP-32 expression and motor coordination performance (Fig. 8B). In contrast, selective CB_1R genetic inactivation in principal cortical neurons (Glu-$CB_1R^{-/-}$ mice) sensitized MSNs to damage induced by astroglial mtHtt expression

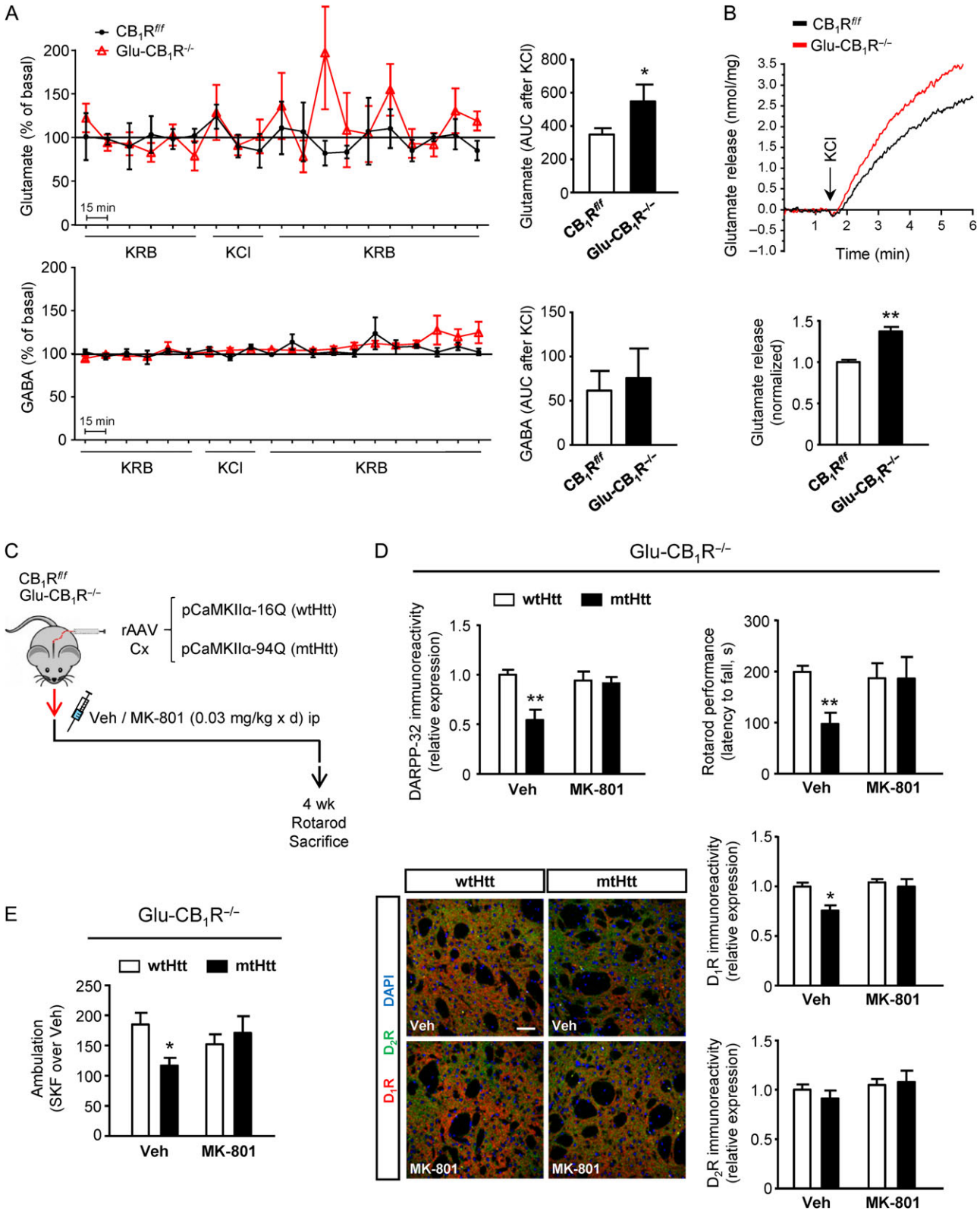

Figure 6. CB_1R located on corticostriatal projections protects D_1R-MSNs from cortical mutant huntingtin-elicited damage by inhibiting glutamatergic transmission. A, Glu-$CB_1R^{-/-}$ mice and $CB_1R^{floxed/floxed}$ littermates were subjected to microdialysis experiments. Glutamate and GABA concentration was measured in dorsal-striatum dialysates. KCl was used at 75 mM. Data are presented as percentage of basal glutamate release of each experiment. *$P < 0.05$ from the corresponding $CB_1R^{floxed/floxed}$ group ($n = 6$ animals per group). B, Striatal synaptosomes were isolated from Glu-$CB_1R^{-/-}$ mice and $CB_1R^{floxed/floxed}$ littermates. Glutamate release in the extracellular medium as induced by 30 mM KCl was measured. **$P < 0.01$ from the corresponding $CB_1R^{floxed/floxed}$ group ($n = 5$–6 animals per group). C-E, Glu-$CB_1R^{-/-}$ mice and $CB_1R^{floxed/floxed}$ littermates were injected stereotactically into the motor cortex with rAAV vectors encoding wtHtt (16Q-CFP) or mtHtt (94Q-CFP) under the control of a CaMKIIα promoter. Animals were subsequently treated with vehicle or MK-801 (0.03 mg/kg/day, i.p.) for 4 weeks. No significant effect was observed in any of the parameters

(Fig. 8B). We next tested whether cortical CB_1R protected MSNs from astroglial mtHtt-induced damage by blunting glutamatergic signaling. For this purpose we injected wild-type C57BL/6N mice with GFAP promoter-driven wtHtt or mtHtt-expressing vectors into the dorsal striatum, and treated them with vehicle or MK-801 (0.03 mg/kg/day, i.p.) for 2 weeks (Fig. 8C). MK-801 administration rescued the loss of striatal DARPP-32 and D_1R expression (Fig. 8D), the decline in RotaRod performance (Fig. 8D), and the impairment of SKF-81297-induced hyperactivity (Fig. 8E) elicited by mtHtt expression in striatal astrocytes.

Taken together, these data support that CB_1R located on corticostriatal projections, by inhibiting glutamatergic transmission, protects D_1R-MSNs not only from cortical mtHtt-evoked damage, as shown above, but also from astroglial mtHtt-evoked damage.

Discussion

A key unanswered question in most neurodegenerative diseases is what molecular factors dictate the selective vulnerability of a particular neuronal population. In the case of HD, the pattern of neurodegeneration is very typical of regional locations and neuronal types in the striatum. Thus, MSNs, especially those found in the dorsal striatum (caudate-putamen), represent the main and earliest cell population altered, whereas, for example, striatal interneurons are typically unaffected or only mildly affected at late stages of the disease (Walker 2007). Many studies based on techniques such as PET, autoradiography, and immunomicroscopy have reported reductions in striatal D_1R and D_2R density in HD patients and animal models. Nonetheless, it is generally believed that D_2R-MSNs are affected at earlier stages of the disease and to a greater extent than D_1R-MSNs, which is consistent with the notion that early-onset chorea-like movements result from a preferential dysfunction/loss of D_2R-MSNs, while later-onset bradykinesia and dystonia are a consequence of an additional dysfunction/loss of D_1R-MSNs (Walker 2007; Han et al. 2010; Ross et al. 2014).

Here, we unveil a new key player in this intricate scenario by showing that CB_1R located on corticostriatal projections, through the control of glutamatergic transmission, dictates a selective protection of D_1R-MSNs from cortical mtHtt-induced damage. CB_1R is one of the most abundant metabotropic receptors in the basal ganglia, where endocannabinoid signaling serves as a major feedback mechanism aimed at preventing excessive presynaptic activity (Glass et al. 2000; Katona and Freund 2008; Atwood et al. 2014). In particular, CB_1R is highly expressed on terminals of both D_1R-MSNs and D_2R-MSNs, where it mediates endocannabinoid-dependent inhibition of GABA release and thus inhibition of motor activity (Katona and Freund 2008; Castillo et al. 2012). CB_1R is also expressed on glutamatergic terminals projecting from the cortex onto the striatum, thereby blunting glutamatergic output and mediating the so-called endocannabinoid-dependent long-term depression (Gerdeman et al. 2002; Kreitzer 2009). This process was initially shown to require D_2R activation and so was proposed to occur exclusively in D_2R-MSNs (Kreitzer and Malenka 2007). However, other findings support that, rather than being specific for D_2R-MSNs, endocannabinoid-dependent long-term depression may exhibit a certain preference to occur at D_2R-MSNs over D_1R-MSNs, and is most likely evoked by different mechanisms in each MSN population (Wang et al. 2006; Bagetta et al. 2011; Mathur and Lovinger 2012; Wu et al. 2015). On anatomical grounds, different cortical excitatory efferents onto D_1R-MSNs and D_2R-MSNs were initially proposed: D_1R-MSNs would receive input preferentially from small, bilateral intratelencephalic projections, while D_2R-MSNs would receive input preferentially from larger, ipsilateral collaterals of the pyramidal tract (Lei et al. 2004; Reiner et al. 2010). However, this idea has been challenged by other morphological and functional studies, in which no significant differences were found regarding the cortical targeting of D_1R-MSNs and D_2R-MSNs (Kress et al. 2013; Silberberg and Bolam 2015). On the other hand, D_1R-MSNs seem to be preferentially innervated by sensory cortical and limbic structures, while the motor cortex could preferentially target D_2R-MSNs (Wall et al. 2013). In any event, excitatory synapses exhibit higher release probability and larger NMDAR currents on D_2R-MSNs than on D_1R-MSNs (Kreitzer and Malenka 2007). Overall, our findings are in line with the notion that CB_1R located on corticostriatal terminals projecting onto D_2R-MSNs could blunt physiological glutamatergic transmission preferentially aimed at controlling D_2R-evoked dopaminergic control of motor behavior. Concertedly, the present study supports that CB_1R located on corticostriatal terminals projecting onto D_1R-MSNs could blunt pathological glutamatergic transmission preferentially aimed at controlling D_1R-evoked dopaminergic neurotoxicity. As D_1R is in excess over D_2R in the striatum, it is plausible that the former will be more significantly activated than the latter upon dopamine spillover (Raymond et al. 2011). On mechanistic grounds, one could speculate that, upon intense activation of glutamatergic projections, glutamate spillover out of the synapse would evoke on targeted D_1R-MSNs the activation of the perisynaptic machinery of endocannabinoid generation, composed of type 1 metabotropic glutamate receptors (mostly $mGluR_5$), heterotrimeric $G_{q/11}$ proteins, phospholipase Cβ, and diacylglycerol lipase-α, thus triggering the production of 2-AG (Uchigashima et al. 2007; Katona and Freund 2008), which would retrogradely engage CB_1R located on glutamatergic terminals, inhibiting in turn excess excitatory transmission (Castillo et al. 2012) and buffering the neurotoxic effects of extrasynaptic NMDA receptors on D_1R-MSNs (Tang et al. 2007; Paoletti et al. 2008; Milnerwood et al. 2009; Okamoto et al. 2009; Chen et al. 2013).

Many studies have dealt with the expression and function of CB_1R in HD. As a matter of fact, HD most likely constitutes the best currently available model disease to assess the pathophysiological relevance and therapeutic potential of CB_1R in neurodegenerative diseases. This is due to at least three important reasons: (1) CB_1R is highly expressed in the dorsal striatum at both MSNs and corticostriatal projections, and plays a key role in the control of motor behavior (the process that is most characteristically affected in HD) (Katona and Freund 2008; Kreitzer 2009; Castillo et al. 2012). (2) We (Blazquez et al. 2011) and others (Mievis et al. 2011) have previously demonstrated a neuroprotective role of CB_1R in transgenic mouse models of HD.

measured in $CB_1R^{floxed/floxed}$ mice, so for clarity only data from Glu-$CB_1R^{-/-}$ animals are shown. C, Scheme of the experiment. D, DARPP-32, D_1R and D_2R immunoreactivity in the dorsal striatum, as well as RotaRod performance (time to fall), in Glu-$CB_1R^{-/-}$ mice. Representative images are shown. Scale bar, 50 μm. Data of neuronal markers are expressed as relative values of the wtHtt-vehicle group. E, After termination of chronic pharmacological treatments and RotaRod assays, ambulation was determined in Glu-$CB_1R^{-/-}$ mice 30 min after a single injection of vehicle or SKF-81297 (1 mg/kg, i.p.). Data are expressed as SKF-81297-induced ambulation over that of vehicle, in cm. *$P < 0.05$, **$P < 0.01$ from the corresponding wtHtt-vehicle group ($n = 6$ animals per group).

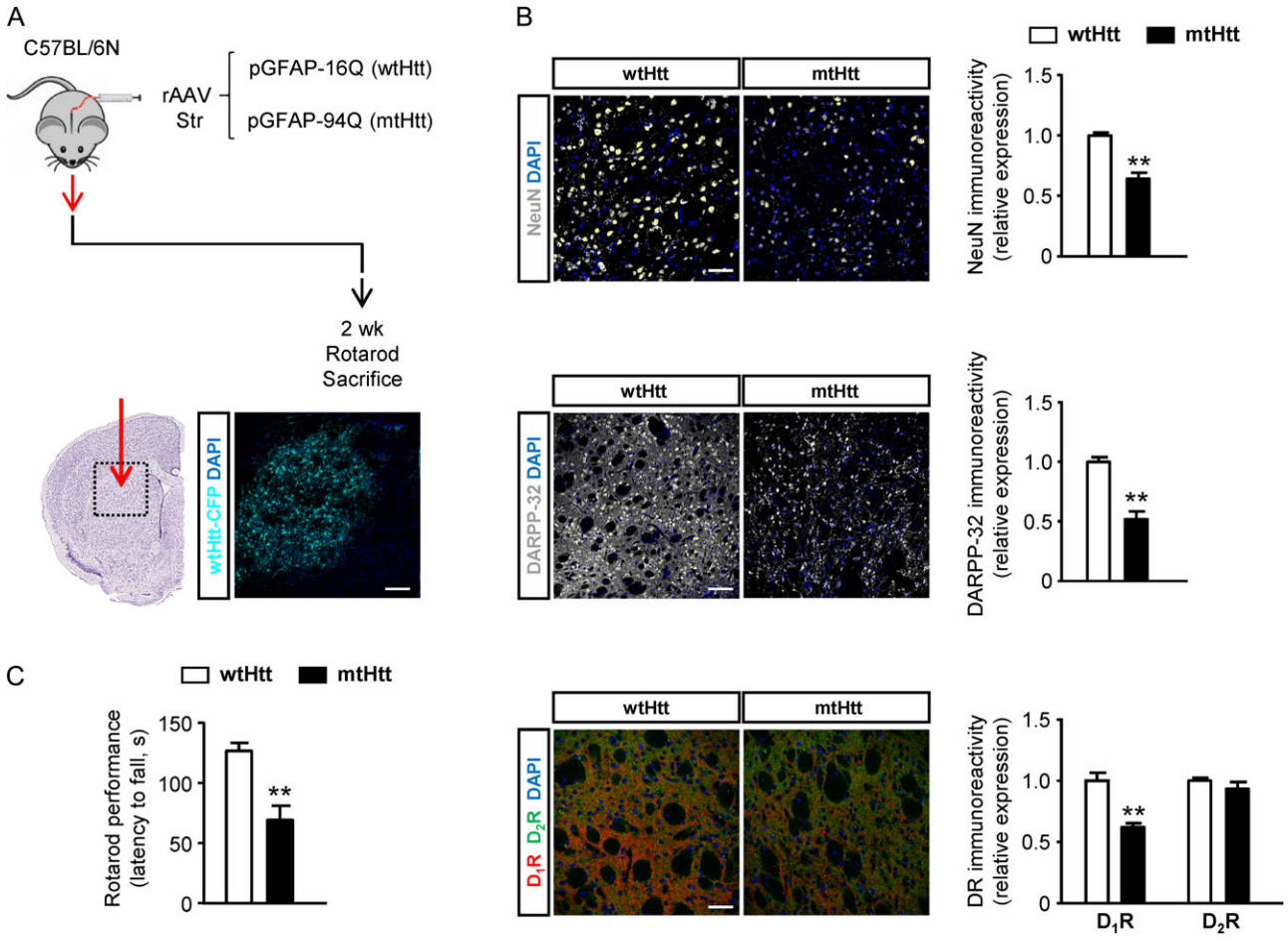

Figure 7. Expression of mutant huntingtin in striatal astrocytes damages D_1R-MSNs. C57BL/6N mice were injected stereotactically into the dorsal striatum with rAAV vectors encoding wtHtt (16Q-CFP) or mtHtt (94Q-CFP) under the control of a GFAP promoter. *A*, Scheme of the experiment. Representative example of a brain hemisphere expressing the wtHtt vector. The dotted line depicts the infected area. Scale bar, 200 μm. *B*, NeuN, DARPP-32, D_1R and D_2R immunoreactivity in the dorsal striatum 2 weeks after viral inoculation. Representative images are shown. Scale bar, 100 μm (upper panel) or 50 μm (middle and lower panels). *C*, RotaRod performance (time to fall) 2 weeks after viral inoculation. Data of neuronal markers are expressed as relative values of the wtHtt group. $^*P < 0.05$, $^{**}P < 0.01$ from the corresponding wtHtt group (n = 8–10 animals per group).

(3) An early and remarkable down-regulation of CB_1R expression has been documented in MSNs from HD patients and animal models (Denovan-Wright and Robertson 2000; Glass et al. 2000; McCaw et al. 2004; Horne et al. 2013). As, in contrast, the expression and function of CB_1R located on corticostriatal projections remains unaffected along HD progression (Chiodi et al. 2012; Chiarlone et al. 2014), it is plausible that the maintenance of CB_1R on corticostriatal projections constitutes an adaptive mechanism aimed at buffering concerted glutamatergic-dopaminergic excitotoxicity on D_1R-MSNs. Nonetheless, it cannot be ruled that other $G_{i/o}$ protein-coupled presynaptic receptors could cooperate with CB_1R in reducing glutamatergic transmission on D_1R-MSNs (Atwood et al. 2014). Evidence obtained from HD patients and mouse models shows that patterns of communication between cortical projections and MSNs become altered from very early, even asymptomatic stages of the disease, thus indicating that a dysfunctional cortical input to the striatum determines the onset and progression of neurological signs (Thu et al. 2010; Ghiglieri et al. 2012; Unschuld et al. 2012; Estrada-Sanchez and Rebec 2013). Likewise, it is generally accepted that MSN dysfunction and associated behavioral deficits in HD are caused by the expression of mtHtt not only in MSNs (cell-autonomous toxicity) but also in cortical pyramidal neurons (non-cell-autonomous toxicity) (Gu et al. 2005; Wang et al. 2014; Estrada-Sanchez et al. 2015). However, it is unknown whether these regional features of mtHtt expression define a potential vulnerability of D_1R-MSNs versus D_2R-MSNs to damage. Here, we show that, regarding the control of MSN survival by the pool of CB_1R molecules located on corticostriatal projections, cortical pyramidal neurons constitute a key site for mtHtt expression to dictate a selective protection of D_1R-MSNs versus D_2R-MSNs. On the other hand, striatal astrocytes are gaining attention as possible contributors to the onset and progression of HD. The implication of astroglial damage in the dysregulation of glutamate and ion homeostasis that occurs in HD has been the focus of recent studies (Tong et al. 2014; Jiang et al. 2016). Our data support that the astrocyte-mediated control of D_1R-MSN integrity does not rely on the engagement of the CB_1R pool located on astrocytes, but on the CB_1R pool located on corticostriatal projections, which, by reducing the release of glutamate into the synaptic cleft, would blunt excitotoxicity. The CB_1R pool located on MSNs could also contribute to controlling the number of corticostriatal connections, but does not seem to be responsible for the motor coordination

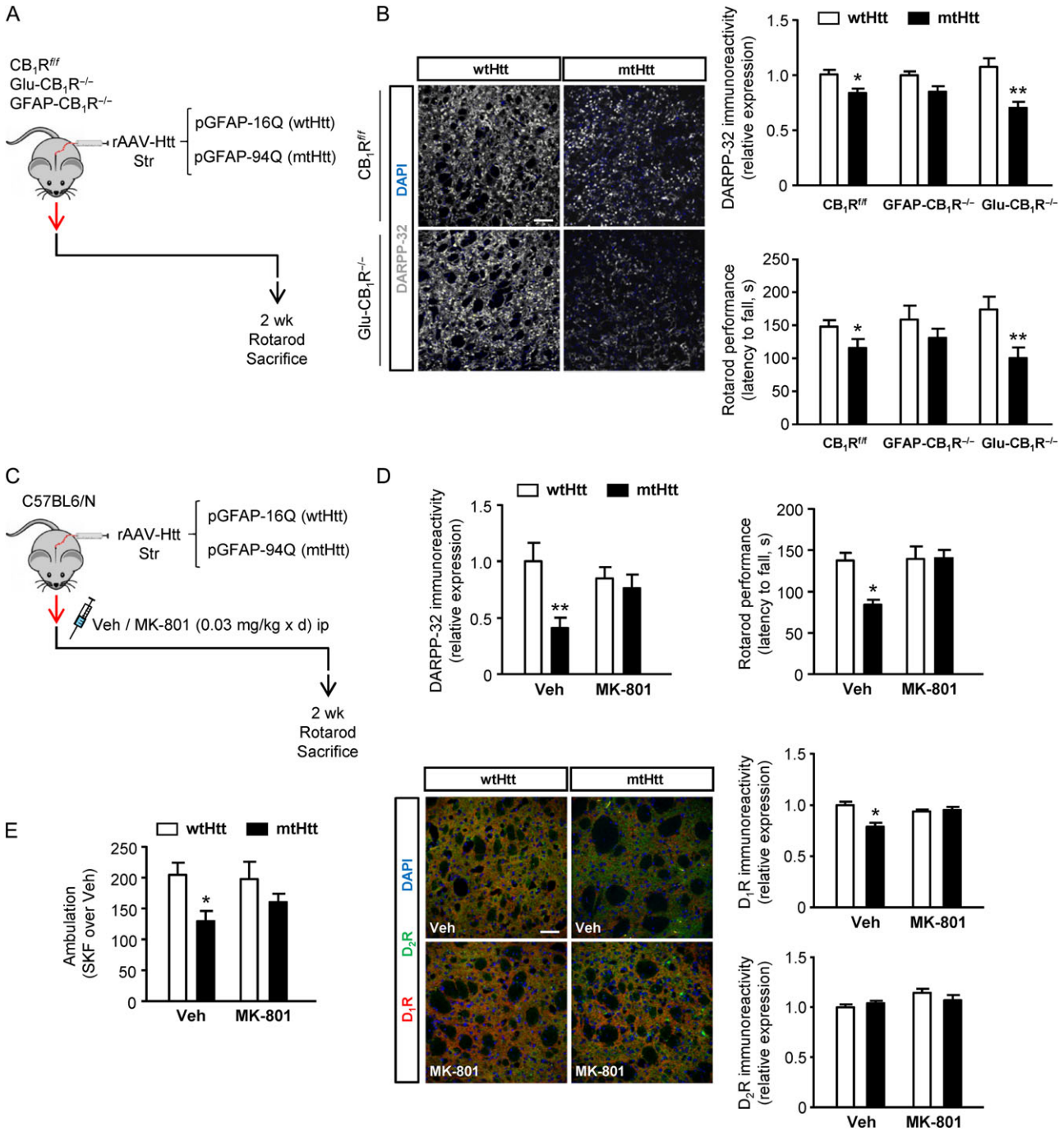

Figure 8. CB_1R located on corticostriatal projections protects D_1R-MSNs from astroglial mutant huntingtin-elicited damage by inhibiting glutamatergic transmission. A–B, GFAP-$CB_1R^{-/-}$ mice, Glu-$CB_1R^{-/-}$ mice and $CB_1R^{floxed/floxed}$ littermates were injected stereotactically into the dorsal striatum with rAAV vectors encoding wtHtt (16Q-CFP) or mtHtt (94Q-CFP) under the control of a GFAP promoter. *A*, Scheme of the experiment. *B*, DARPP-32 immunoreactivity in the dorsal striatum and RotaRod performance (time to fall) 2 weeks after viral inoculation. DARPP-32 data are expressed as relative values of the wtHtt-$CB_1R^{floxed/floxed}$ group. Representative images are shown. Scale bar, 100 μm. *P < 0.05, **P < 0.01 from the corresponding wtHtt group (n = 5–10 animals per group). C–F, C57BL/6 N mice were injected stereotactically into the dorsal striatum with rAAV vectors encoding wtHtt (16Q-CFP) or mtHtt (94Q-CFP) under the control of a GFAP promoter. Animals were subsequently treated with vehicle or MK-801 (0.03 mg/kg/day, i.p.) for 2 weeks. *C*, Scheme of the experiment. *D*, DARPP-32, D_1R and D_2R immunoreactivity in the dorsal striatum, as well as RotaRod performance (time to fall). Representative images are shown. Scale bar, 50 μm. Data of neuronal markers are expressed as relative values of the wtHtt-vehicle group. *E*, After termination of chronic pharmacological treatments and RotaRod assays, ambulation was determined 30 min after a single injection of vehicle or SKF-81297 (1 mg/kg, i.p.). Data are expressed as SKF-81297-induced ambulation over that of vehicle, in cm. *P < 0.05, **P < 0.01 from the corresponding wtHtt-vehicle group (n = 6–8 animals per group).

deficits occurring in mouse models of HD (Chiarlone et al. 2014; Naydenov et al. 2014). Taken together, these findings add to the current view of how non-cell-autonomous mtHtt actions orchestrate complex alterations on D_1R-MSNs versus D_2R-MSNs, and may help to understand the intricate pathophysiology of basal ganglia disorders.

Supplementary Material

Supplementary data are available at *Cerebral Cortex* online.

Funding

The Spanish *Ministerio de Economía y Competitividad* (MINECO/FEDER; grant numbers SAF2015-64945-R to M.G., RTC2015-3364-1 to I.G.-R., SAF2013-45570-R to J.A.R.-N. and BFU 2013-43163-R to J.S.-P.). J.A.R.-N. was also supported by the Spanish *Instituto de Salud Carlos III* (ISCIII/FEDER, grant number CP13-00234). A.R.-C. and A.G. were supported by contracts from the Spanish *Ministerio de Economía y Competitividad* (MINECO/FEDER; *Formación de Personal Investigador* Program). I.B.M. was supported by a contract from the Spanish *Ministerio de Educación, Cultura y Deporte* (*Formación de Personal Universitario* Program). G.M. and L. B. were supported by *Institut National de la Santé et de la Recherche Médicale*. G.M. was also supported by EU–Fp7 (PAINCAGE, grant number HEALTH-603191), *Fondation pour la Recherche Medicale* (grant numbers DRM20101220445 and DPP20151033974), Human Frontiers Science Program (grant number RGP0036/2014), European Research Council (Endofood grant number ERC–2010–StG–260515, and CannaPreg grant number ERC-2014-PoC-640923), *Region Nouvelle Aquitaine*, and *Agence Nationale de la Recherche* (ANR Blanc NeuroNutriSens grant number ANR-13-BSV4-0006, BRAIN grant number ANR-10-LABX-0043, and ANR Blanc ORUPS grant number ANR-16-CE37-0010-01). L.B. was also supported by European Molecular Biology Organization (grant number ALTF 975-2011) and *Fondation pour la Recherche Medicale* (grant number ARF20140129235).

Notes

We are indebted to R. Moratalla for providing the *Drd1a*-tdTomato/*Drd2*-EGFP mouse colony founders; J.J. Lucas for providing the Htt-CFP plasmids; B.L. Roth for providing the hM3Dq-mCherry plasmid; and K. Deisseroth for providing the CaMKIIα promoter plasmid. We also thank E. García-Taboada, A. Sánchez-Herranz, P. García-Rozas, and M.J. Asensio for expert laboratory assistance; D. Gonzales, N. Aubailly, and all the personnel from the animal facilities of the NeuroCentre Magendie; M. Biguerie from the technical service of the NeuroCentre Magendie; all the personnel from the Bordeaux Imaging Center; and V. Morales for continuous help. *Conflict of Interest*: The authors declare no competing financial interests.

References

Alexander GM, Rogan SC, Abbas AI, Armbruster BN, Pei Y, Allen JA, Nonneman RJ, Hartmann J, Moy SS, Nicolelis MA, et al. 2009. Remote control of neuronal activity in transgenic mice expressing evolved G protein-coupled receptors. Neuron. 63:27–39.

Andre VM, Fisher YE, Levine MS. 2011. Altered balance of activity in the striatal direct and indirect pathways in mouse models of Huntington's disease. Front Syst Neurosci. 5:46.

Atwood BK, Lovinger DM, Mathur BN. 2014. Presynaptic long-term depression mediated by Gi/o-coupled receptors. Trends Neurosci. 37:663–673.

Bagetta V, Picconi B, Marinucci S, Sgobio C, Pendolino V, Ghiglieri V, Fusco FR, Giampa C, Calabresi P. 2011. Dopamine-dependent long-term depression is expressed in striatal spiny neurons of both direct and indirect pathways: implications for Parkinson's disease. J Neurosci. 31:12513–12522.

Bellocchio L, Ruiz-Calvo A, Chiarlone A, Cabanas M, Resel E, Cazalets JR, Blazquez C, Cho YH, Galve-Roperh I, Guzman M. 2016. Sustained Gq-protein signaling disrupts striatal circuits via JNK. J Neurosci. 36:10611–10624.

Benraiss A, Wang S, Herrlinger S, Li X, Chandler-Militello D, Mauceri J, Burm HB, Toner M, Osipovitch M, Jim Xu Q, et al. 2016. Human glia can both induce and rescue aspects of disease phenotype in Huntington disease. Nat Commun. 7:11758.

Blazquez C, Chiarlone A, Bellocchio L, Resel E, Pruunsild P, Garcia-Rincon D, Sendtner M, Timmusk T, Lutz B, Galve-Roperh I, et al. 2015. The CB_1 cannabinoid receptor signals striatal neuroprotection via a PI3K/Akt/mTORC1/BDNF pathway. Cell Death Differ. 22:1618–1629.

Blazquez C, Chiarlone A, Sagredo O, Aguado T, Pazos MR, Resel E, Palazuelos J, Julien B, Salazar M, Borner C, et al. 2011. Loss of striatal type 1 cannabinoid receptors is a key pathogenic factor in Huntington's disease. Brain. 134:119–136.

Castillo PE, Younts TJ, Chavez AE, Hashimotodani Y. 2012. Endocannabinoid signaling and synaptic function. Neuron. 76:70–81.

Cepeda C, Levine MS. 1998. Dopamine and N-methyl-D-aspartate receptor interactions in the neostriatum. Dev Neurosci. 20: 1–18.

Chen JY, Wang EA, Cepeda C, Levine MS. 2013. Dopamine imbalance in Huntington's disease: a mechanism for the lack of behavioral flexibility. Front Neurosci. 7:114.

Chiarlone A, Bellocchio L, Blazquez C, Resel E, Soria-Gomez E, Cannich A, Ferrero JJ, Sagredo O, Benito C, Romero J, et al. 2014. A restricted population of CB_1 cannabinoid receptors with neuroprotective activity. Proc Natl Acad Sci USA. 111: 8257–8262.

Chiodi V, Uchigashima M, Beggiato S, Ferrante A, Armida M, Martire A, Potenza RL, Ferraro L, Tanganelli S, Watanabe M, et al. 2012. Unbalance of CB_1 receptors expressed in GABAergic and glutamatergic neurons in a transgenic mouse model of Huntington's disease. Neurobiol Dis. 45:983–991.

Denovan-Wright EM, Robertson HA. 2000. Cannabinoid receptor messenger RNA levels decrease in a subset of neurons of the lateral striatum, cortex and hippocampus of transgenic Huntington's disease mice. Neuroscience. 98:705–713.

Estrada-Sanchez AM, Burroughs CL, Cavaliere S, Barton SJ, Chen S, Yang XW, Rebec GV. 2015. Cortical efferents lacking mutant huntingtin improve striatal neuronal activity and behavior in a conditional mouse model of Huntington's disease. J Neurosci. 35:4440–4451.

Estrada-Sanchez AM, Rebec GV. 2013. Role of cerebral cortex in the neuropathology of Huntington's disease. Front Neural Circuits. 7:19.

Fernandez-Ruiz J, Moreno-Martet M, Rodriguez-Cueto C, Palomo-Garo C, Gomez-Canas M, Valdeolivas S, Guaza C, Romero J, Guzman M, Mechoulam R, et al. 2011. Prospects for cannabinoid therapies in basal ganglia disorders. Br J Pharmacol. 163:1365–1378.

Gerdeman GL, Ronesi J, Lovinger DM. 2002. Postsynaptic endocannabinoid release is critical to long-term depression in the striatum. Nat Neurosci. 5:446–451.

Ghiglieri V, Bagetta V, Calabresi P, Picconi B. 2012. Functional interactions within striatal microcircuit in animal models of Huntington's disease. Neuroscience. 211:165–184.

Glass M, Dragunow M, Faull RL. 2000. The pattern of neurodegeneration in Huntington's disease: a comparative study of cannabinoid, dopamine, adenosine and $GABA_A$ receptor alterations in the human basal ganglia in Huntington's disease. Neuroscience. 97:505–519.

Go BS, Ahn SM, Shim I, Choe ES. 2010. Activation of c-Jun N-terminal kinase is required for the regulation of endoplasmic

reticulum stress response in the rat dorsal striatum following repeated cocaine administration. Neuropharmacology. 59:100–106.

Gomez JL, Bonaventura J, Lesniak W, Mathews WB, Sysa-Shah P, Rodriguez LA, Ellis RJ, Richie CT, Harvey BK, Dannals RF, et al. 2017. Chemogenetics revealed: DREADD occupancy and activation via converted clozapine. Science. 357:503–507.

Gu X, Li C, Wei W, Lo V, Gong S, Li SH, Iwasato T, Itohara S, Li XJ, Mody I, et al. 2005. Pathological cell-cell interactions elicited by a neuropathogenic form of mutant Huntingtin contribute to cortical pathogenesis in HD mice. Neuron. 46:433–444.

Han I, You Y, Kordower JH, Brady ST, Morfini GA. 2010. Differential vulnerability of neurons in Huntington's disease: the role of cell type-specific features. J Neurochem. 113:1073–1091.

Han J, Kesner P, Metna-Laurent M, Duan T, Xu L, Georges F, Koehl M, Abrous DN, Mendizabal-Zubiaga J, Grandes P, et al. 2012. Acute cannabinoids impair working memory through astroglial CB_1 receptor modulation of hippocampal LTD. Cell. 148:1039–1050.

Hedreen JC, Folstein SE. 1995. Early loss of neostriatal striosome neurons in Huntington's disease. J Neuropath Exp Neur. 54: 105–120.

Horne EA, Coy J, Swinney K, Fung S, Cherry AE, Marrs WR, Naydenov AV, Lin YH, Sun X, Keene CD, et al. 2013. Downregulation of cannabinoid receptor 1 from neuropeptide Y interneurons in the basal ganglia of patients with Huntington's disease and mouse models. Eur J Neurosci. 37: 429–440.

Jansen AH, van Hal M, Op den Kelder IC, Meier RT, de Ruiter AA, Schut MH, Smith DL, Grit C, Brouwer N, Kamphuis W, et al. 2017. Frequency of nuclear mutant huntingtin inclusion formation in neurons and glia is cell-type-specific. Glia. 65:50–61.

Jayanthi S, McCoy MT, Ladenheim B, Cadet JL. 2002. Methamphetamine causes coordinate regulation of Src, Cas, Crk, and the Jun N-terminal kinase-Jun pathway. Mol Pharmacol. 61:1124–1131.

Jiang R, Diaz-Castro B, Looger LL, Khakh BS. 2016. Dysfunctional calcium and glutamate signaling in striatal astrocytes from Huntington's disease model mice. J Neurosci. 36:3453–3470.

Katona I, Freund TF. 2008. Endocannabinoid signaling as a synaptic circuit breaker in neurological disease. Nat Med. 14: 923–930.

Kreitzer AC. 2009. Physiology and pharmacology of striatal neurons. Annu Rev Neurosci. 32:127–147.

Kreitzer AC, Malenka RC. 2007. Endocannabinoid-mediated rescue of striatal LTD and motor deficits in Parkinson's disease models. Nature. 445:643–647.

Kress GJ, Yamawaki N, Wokosin DL, Wickersham IR, Shepherd GM, Surmeier DJ. 2013. Convergent cortical innervation of striatal projection neurons. Nat Neurosci. 16:665–667.

Lee HM, Giguere PM, Roth BL. 2014. DREADDs: novel tools for drug discovery and development. Drug Discov Today. 19: 469–473.

Lei W, Jiao Y, Del Mar N, Reiner A. 2004. Evidence for differential cortical input to direct pathway versus indirect pathway striatal projection neurons in rats. J Neurosci. 24:8289–8299.

Martin R, Durroux T, Ciruela F, Torres M, Pin JP, Sanchez-Prieto J. 2010. The metabotropic glutamate receptor mGlu7 activates phospholipase C, translocates munc-13-1 protein, and potentiates glutamate release at cerebrocortical nerve terminals. J Biol Chem. 285:17907–17917.

Mathur BN, Lovinger DM. 2012. Endocannabinoid-dopamine interactions in striatal synaptic plasticity. Front Pharmacol. 3:66.

Maynard CJ, Bottcher C, Ortega Z, Smith R, Florea BI, Diaz-Hernandez M, Brundin P, Overkleeft HS, Li JY, Lucas JJ, et al. 2009. Accumulation of ubiquitin conjugates in a polyglutamine disease model occurs without global ubiquitin/proteasome system impairment. Proc Natl Acad Sci USA. 106:13986–13991.

McCaw EA, Hu H, Gomez GT, Hebb AL, Kelly ME, Denovan-Wright EM. 2004. Structure, expression and regulation of the cannabinoid receptor gene (CB_1) in Huntington's disease transgenic mice. Eur J Biochem. 271:4909–4920.

McLaughlin BA, Nelson D, Erecinska M, Chesselet MF. 1998. Toxicity of dopamine to striatal neurons in vitro and potentiation of cell death by a mitochondrial inhibitor. J Neurochem. 70:2406–2415.

Meunier C, Merienne N, Jolle C, Deglon N, Pellerin L. 2016. Astrocytes are key but indirect contributors to the development of the symptomatology and pathophysiology of Huntington's disease. Glia. 64:1841–1856.

Mievis S, Blum D, Ledent C. 2011. Worsening of Huntington disease phenotype in CB_1 receptor knockout mice. Neurobiol Dis. 42:524–529.

Milnerwood AJ, Gladding CM, Pouladi MA, Kaufman AM, Hines RM, Boyd JD, Ko RW, Vasuta OC, Graham RK, Hayden MR, et al. 2009. Early increase in extrasynaptic NMDA receptor signaling and expression contributes to phenotype onset in Huntington's disease mice. Neuron. 65:178–190.

Mitchell IJ, Griffiths MR. 2003. The differential susceptibility of specific neuronal populations: insights from Huntington's disease. IUBMB Life. 55:293–298.

Monory K, Massa F, Egertova M, Eder M, Blaudzun H, Westenbroek R, Kelsch W, Jacob W, Marsch R, Ekker M, et al. 2006. The endocannabinoid system controls key epileptogenic circuits in the hippocampus. Neuron. 51:455–466.

Murphy-Royal C, Dupuis J, Groc L, Oliet SH. 2017. Astroglial glutamate transporters in the brain: Regulating neurotransmitter homeostasis and synaptic transmission. J Neurosci Res. 95:2140–2151.

Navarrete M, Araque A. 2010. Endocannabinoids potentiate synaptic transmission through stimulation of astrocytes. Neuron. 68:113–126.

Naydenov AV, Sepers MD, Swinney K, Raymond LA, Palmiter RD, Stella N. 2014. Genetic rescue of CB_1 receptors on medium spiny neurons prevents loss of excitatory striatal synapses but not motor impairment in HD mice. Neurobiol Dis. 71:140–150.

Okamoto SI, Pouladi MA, Talantova M, Yao D, Xia P, Ehrnhoefer DE, Zaidi R, Clemente A, Kaul M, Graham RK, et al. 2009. Balance between synaptic versus extrasynaptic NMDA receptor activity influences inclusions and neurotoxicity of mutant huntingtin. Nat Med. 15:1407–1413.

Paoletti P, Vila I, Rife M, Lizcano JM, Alberch J, Gines S. 2008. Dopaminergic and glutamatergic signaling crosstalk in Huntington's disease neurodegeneration: the role of p25/cyclin-dependent kinase 5. J Neurosci. 28:10090–10101.

Raymond LA, Andre VM, Cepeda C, Gladding CM, Milnerwood AJ, Levine MS. 2011. Pathophysiology of Huntington's disease: time-dependent alterations in synaptic and receptor function. Neuroscience. 198:252–273.

Reiner A, Hart NM, Lei W, Deng Y. 2010. Corticostriatal projection neurons - dichotomous types and dichotomous functions. Front Neuroanat. 4:142.

Rikani AA, Choudhry Z, Choudhry AM, Rizvi N, Ikram H, Mobassarah NJ, Tulli S. 2014. The mechanism of degeneration of striatal neuronal subtypes in Huntington disease. Ann Neurosci. 21:112–114.

Rodriguez-Navarro JA, Gonzalo-Gobernado R, Herranz AS, Gonzlez-Vigueras JM, Solis JM. 2009. High potassium induces taurine release by osmosensitive and osmoresistant mechanisms in the rat hippocampus in vivo. J Neurosci Res. 87:208–217.

Ross CA, Aylward EH, Wild EJ, Langbehn DR, Long JD, Warner JH, Scahill RI, Leavitt BR, Stout JC, Paulsen JS, et al. 2014. Huntington disease: natural history, biomarkers and prospects for therapeutics. Nat Rev Neurol. 10:204–216.

Sepers MD, Raymond LA. 2014. Mechanisms of synaptic dysfunction and excitotoxicity in Huntington's disease. Drug Discov Today. 19:990–996.

Silberberg G, Bolam JP. 2015. Local and afferent synaptic pathways in the striatal microcircuitry. Curr Opin Neurobiol. 33: 182–187.

Stella N. 2010. Cannabinoid and cannabinoid-like receptors in microglia, astrocytes, and astrocytomas. Glia. 58:1017–1030.

Suarez LM, Solis O, Carames JM, Taravini IR, Solis JM, Murer MG, Moratalla R. 2014. L-DOPA treatment selectively restores spine density in dopamine receptor D2-expressing projection neurons in dyskinetic mice. Biol Psychiatry. 75: 711–722.

Tang TS, Chen X, Liu J, Bezprozvanny I. 2007. Dopaminergic signaling and striatal neurodegeneration in Huntington's disease. J Neurosci. 27:7899–7910.

Thu DC, Oorschot DE, Tippett LJ, Nana AL, Hogg VM, Synek BJ, Luthi-Carter R, Waldvogel HJ, Faull RL. 2010. Cell loss in the motor and cingulate cortex correlates with symptomatology in Huntington's disease. Brain. 133:1094–1110.

Tong X, Ao Y, Faas GC, Nwaobi SE, Xu J, Haustein MD, Anderson MA, Mody I, Olsen ML, Sofroniew MV, et al. 2014. Astrocyte Kir4.1 ion channel deficits contribute to neuronal dysfunction in Huntington's disease model mice. Nat Neurosci. 17:694–703.

Uchigashima M, Narushima M, Fukaya M, Katona I, Kano M, Watanabe M. 2007. Subcellular arrangement of molecules for 2-arachidonoyl-glycerol-mediated retrograde signaling and its physiological contribution to synaptic modulation in the striatum. J Neurosci. 27:3663–3676.

Unschuld PG, Joel SE, Liu X, Shanahan M, Margolis RL, Biglan KM, Bassett SS, Schretlen DJ, Redgrave GW, van Zijl PC, et al. 2012. Impaired cortico-striatal functional connectivity in prodromal Huntington's Disease. Neurosci Lett. 514:204–209.

Walker FO. 2007. Huntington's disease. Lancet. 369:218–228.

Wall NR, De La Parra M, Callaway EM, Kreitzer AC. 2013. Differential innervation of direct- and indirect-pathway striatal projection neurons. Neuron. 79:347–360.

Wang N, Gray M, Lu XH, Cantle JP, Holley SM, Greiner E, Gu X, Shirasaki D, Cepeda C, Li Y, et al. 2014. Neuronal targets for reducing mutant huntingtin expression to ameliorate disease in a mouse model of Huntington's disease. Nat Med. 20:536–541.

Wang Z, Kai L, Day M, Ronesi J, Yin HH, Ding J, Tkatch T, Lovinger DM, Surmeier DJ. 2006. Dopaminergic control of corticostriatal long-term synaptic depression in medium spiny neurons is mediated by cholinergic interneurons. Neuron. 50:443–452.

Wu YW, Kim JI, Tawfik VL, Lalchandani RR, Scherrer G, Ding JB. 2015. Input- and cell-type-specific endocannabinoid-dependent LTD in the striatum. Cell Rep. 10:75–87.

Zeron MM, Hansson O, Chen N, Wellington CL, Leavitt BR, Brundin P, Hayden MR, Raymond LA. 2002. Increased sensitivity to N-methyl-D-aspartate receptor-mediated excitotoxicity in a mouse model of Huntington's disease. Neuron. 33:849–860.